PLANT PHYSIOLOGY AND BIOCHEMISTRY 125 (2018): 153-163

DOI: https://doi.org/10.1016/j.plaphy.2018.01.033

Silicon induced Fe deficiency affects Fe, Mn, Cu and Zn distribution in rice (*Oryza sativa* L.) growth in calcareous conditions

Sandra Carrasco-Gil[a*], Sara Rodríguez-Menéndez[b], Beatriz Fernández[b], Rosario Pereiro[b], Vicenta de la Fuente[c] and Lourdes Hernandez-Apaolaza[a]

[a]*Department of Agricultural Chemistry and Food Science. Universidad Autónoma de Madrid, Av. Francisco Tomás y Valiente 7, 28049 Madrid, Spain*

[b]*Department of Physical and Analytical Chemistry, Facultad de Química, Universidad de Oviedo, Julian Clavería, 8, E-33006 Oviedo, Spain*

[c]*Department of Biology. Universidad Autónoma de Madrid, Calle Darwin 2, 28049 Madrid, Spain*

**Corresponding author:* sandra.carrasco@uam.es (S. Carrasco-Gil);

lourdes.hernandez@uam.es (L. Hernández-Apaolaza)

Abstract

A protective effect by silicon in the amelioration of iron chlorosis has recently been proved for Strategy 1 species, at acidic pH. However in calcareous conditions, the Si effect on Fe acquisition and distribution is still unknown. In this work, the effect of Si on Fe, Mn, Cu and Zn distribution was studied in rice (Strategy 2 species) under Fe sufficiency and deficiency. Plants (+Si or-Si) were grown initially with Fe, and then Fe was removed from the nutrient solution. The plants were then analysed using a combined approach including LA-ICP-MS images for each element of interest, the analysis of the Fe and Si concentration at different cell layers of root and leaf cross sections by SEM-EDX, and determining the apoplastic Fe, total micronutrient concentration and oxidative stress indexes. A different Si effect was observed depending on plant Fe status. Under Fe sufficiency, Si supply increased Fe root plaque formation, decreasing Fe concentration inside the root and increasing the oxidative stress in the plants. Therefore, Fe acquisition strategies were activated, and Fe translocation rate to the aerial parts was increased, even under an optimal Fe supply. Under Fe deficiency, +Si plants absorbed Fe from the plaque more rapidly than –Si plants, due to the previous activation of Fe deficiency strategies during the growing period (+Fe+Si). Higher Fe plaque formation due to Si supply during the growing period reduced Fe uptake and could activate Fe deficiency strategies in rice, making it more efficient against Fe chlorosis alterations. Silicon influenced Mn and Cu distribution in root.

Key words: rice **(***Oryza sativa* L.), silicon, iron-deficiency, iron-localization, micronutrients distribution.

1. Introduction

Among the grass species, rice is one of the crops most susceptible to Fe deficiency, especially during the early stages of plant development in calcareous soils (pH > 7.5). At such pH, available Fe in the soil is limited for plant optimal growth so deficiency symptoms appear, and crop yield and quality could be severely reduced. To overcome Fe deficiency, efficient plants develop different strategies. Dicots and non-graminaceous plants increase the roots' Fe(III) reduction power through an Fe(III)-chelate reductase coupled with an increase in the biosynthesis of a Fe(II) transporter; rhizosphere acidification and the release of phenolic compounds have also been described as tools to increase the available Fe in the rhizosphere (Strategy I). Graminaceous plants (Strategy II) release specific Fe chelating agents, called phytosiderophores (PS), to the rhizosphere in order to solubilize Fe from the soils. The two strategies outlined above are not exclusive, and rice (*Oryza sativa* L.) employs both strategies (Ishimaru et al., 2006).

Rice is a Si-accumulating plant species (Ma et al., 2006), and the major form of Si in the xylem has been identified as monomeric silicic acid, which is further concentrated through loss of water (transpiration) and polymerized (> 90%) in the form of silica gel. Silicon's protective effect in the amelioration of Fe chlorosis has recently been proven for Strategy 1 species, such as soybean and cucumber (Gonzalo et al., 2013; Pavlovic et al., 2013; Bityutskii et al., 2014; Pavlovic et al., 2016). In cucumber, Pavlovic et al., (2013) demonstrated that the application of Si increased the root apoplastic Fe pool and enhanced the expression of proteins involved in reduction-based Fe uptake. Moreover, Si influenced the gene expression involved in the biosynthesis of Fe-mobilizing compounds, thus resulting in enhanced accumulation of organic acids and phenolics which mediate increased Fe availability in the rhizosphere and mobilization of root apoplastic Fe (Pavlovic et al., 2013). It has also been shown for that crop, that application of Si can facilitate mobility and xylem translocation of Fe towards the shoot, along with the accumulation of Fe-chelating compounds, such as citrate, in xylem sap and leaf tissues (Pavlovic et al., 2013; Bityutskii et al., 2014). However, Si's effect on iron plant nutrition under Fe deficiency stress conditions clearly depends on the plant species (Gonzalo et al., 2013), possibly due to the great differences observed in the Si accumulation pattern among species and on mechanisms developed to overcome the

metal deficiency situations. Nevertheless, the mechanism that explains the role of Si in Fe transport from root to shoot is still unclear (Hernández-Apaolaza, 2014).

An important tool in plant nutrition research is the visualization of element distribution at different scales from the tissue to subcellular levels. This spatial information provides important clues to understanding the mechanisms of regulation of the homeostasis of essential and toxic minerals. Although numerous studies have investigated the cellular distributions of macronutrients or metals/metalloids in hyperaccumulator plants, visualization of trace elements in plant cells of nonhyperaccumulator species is more challenging because of their low concentrations (Moore et al., 2014). Novel imaging techniques such as synchrotron-based X-ray fluorescence (S-XRF), secondary ion mass spectrometry (nanoSIMS), and laser-ablation inductively coupled plasma mass spectrometry (LA-ICP-MS) offer greater sensitivity and spatial resolution, suitable for trace element determination in plant tissues.

For specifically visualizing ferric Fe in plants, Perls staining is one of the oldest methods used (Roschzttardtz et al., 2009) because of its specificity, low-cost, and simplicity. Other techniques such as transmission electron microscopy (TEM) or scanning electron microscopy (SEM) have been used to create a 2-dimensional representation of organelle position in relation to Fe dispersion (Lanquar et al., 2005), resulting in high resolution *in situ* elemental maps. Furthermore, if energy-dispersive X-ray analysis (EDX or EDAX) is used, the Fe distribution in the tissue could be described. The large majority of the available information related to the localization of Fe, Mn, Cu, Zn and Si in rice is focused on rice seeds using S-XRF (Lu et al., 2013). However, a few studies have focused on the rice plant tissue. Moore et al., (2014) investigated the cellular and subcellular localization of Fe, Mn, Cu, Zn and Si in node, internode and leaf sheath of rice using S-XRF and nanoSIMS. They reported that Cu and Si were generally localized in the cell wall, in the case of Si concretely in the cell wall of the parenchyma and the phloem of the vascular bundles. Fe and Zn were strongly localized in the vacuoles of specific cell types, and Mn was localized in the parenchyma cells. Other studies focused on the roots of rice plants reported that Fe was only localized in the epidermis of the root with a nonhomogeneous distribution (Moore et al., 2011), and Si was localized in characteristic rings in the epidermal and endodermal cell walls (Gong et al., 2006; Moore et al., 2011).

The aim of this work was to evaluate the possible effect of Si on Fe distribution in rice when this element was suppressed from the nutrient solution using SEM-EDX and LA-ICP-MS techniques for elemental localization. The distribution of other micronutrients (Mn, Cu, and Zn) was also evaluated. To our knowledge, this is the first time that high resolution images of micronutrients (Fe, Mn, Cu, and Zn) have been obtained for plants under different Fe status.

2. Material and Methods

2.1. Plant material and experimental design

Rice (*Oryza sativa* L. cv. Marisma) plants were grown in a growth chamber with a photosynthetic photon flux density at leaf height of 1000 μmol m^{-2} s^{-1} photosynthetically active radiation, 16-h, 25 °C, 40% humidity (day) and 8-h, 20 °C, 60% humidity (night). Rice seeds (generously provided by Arrozúa S.C.) were sterilized with sodium hypochlorite (20%) and Tween 80 (0.1%) and germinated on filter moistened paper with distilled water for one week in the dark at 28 ºC. Homogeneous seedlings were transferred to 1.6 L plastic boxes containing full-strength nutrient solution (in mM: 1 $Ca(NO_3)_2$, 0.9 KNO_3, 0.3 Mg SO_4, 0.1 KH_2PO_4, 0.035 NaCl, 0.010 H_3BO_3, 0.00005 Na_2MoO_4, 0.001 $MnSO_4$, 0.0005 $CuSO_4$, 0.0005 $ZnSO_4$, 0.0001 $NiCl_2$, 0.0001 $CoSO_4$) with 60 μM Fe-EDTA and 1.5 mM H_4SiO_4 (+Si treatment) or 0 mM H_4SiO_4 (–Si treatment) freshly prepared for 10 days. The pH was fixed at 7.5 by the addition of 3 mM HEPES and readjusted every day. After that, half the +Si plants and half the –Si plants were transferred to nutrient solution without Fe-EDTA (-Fe) and the rest of material continued with 60 μM Fe-EDTA (+Fe) for 4 days more. The nutrient solution was renewed every 4 days. Three biological replicates (+Fe+Si; +Fe-Si; -Fe+Si, -Fe-Si) were performed per treatment.

Prior to analysis, roots and leaves were washed with 0.3 % HCl (v/v) and 0.1% Tween 80 and rinsed twice with distilled water.

2.2. Micronutrient concentration in plant tissue

Plant sampling was performed four days after the Fe-deficiency induction (21 days-old plants). To obtain the dry weights (DW), plants were oven dried at 60 °C to constant weight. For micronutrient analysis, plant samples (0.1-0.3 g DW) were digested with 8

mL HNO_3 (65%), 2 mL H_2O_2 (30%), and 1 mL HF (40%), using a microwave (CEM Corporation MARS 240/50, Matthews, NC, USA) following the procedure described by Gonzalo et al., (2013). All reagents used were Suprapur grade (Merk KGaA, Darmstadt, Germany). Samples were then filtered through a 0.20-µm paper filter and made up to 20 mL with deionized water (type I reagent grade). Total Fe, Mn, Cu, and Zn concentrations were determined by atomic absorption spectrometry using a Perkin-Elmer AAnalyst TM 800 instrument (Perkin Elmer, Waltham, MA, USA). The ratio between micronutrient concentration in leaves and root was calculated.

2.3. Fe concentration in root apoplast and root apoplast Fe free tissue of rice plants

The Fe concentration in root apoplast was analysed at day 1, 4 and 7 after the removal of Fe from the nutrient solution following the procedure described by Bienfait et al., (1985) with some modifications. Intact Fe-deficient roots of each treatment were washed in a solution containing 0.5 mM $CaSO_4$ and 5 mM MES for 10 min. Then roots were transferred to 21 mL of incubation solution containing 5 mM MES (pH 5.5), 0.5 mM $CaSO_4$, and 1.5 mM 2,2′-bipyridyl and incubated for 10 min under reductive conditions by adding 0.5 g solid Na-dithionite under continuous N_2 bubbling. The red Fe^{II} $(bipyridyl)_3$ complex was determined at 520 nm using an extinction coefficient of 8.65 mM^{-1}. After that, rice roots were washed as described, and Fe concentration in the Fe apoplastic free tissue was determined by atomic absorption spectrometry, following the procedure described above.

2.4. 2-D image of Fe, Mn, Cu and Zn localization using laser ablation-ICP-MS

Fresh roots of 21 day-old plants were washed and blotted dry with filter paper. Then, root pieces (1 cm length) cut at five cm from root tip were embedded in 2% plant-agar (Duchefa Biochemie, Haarlem, Netherlands) and sectioned transversally (200 µm thickness) using a vibrating blade microtome (VT1200S Leica Microsystem GmbH, Wetzlar, Germany). Fresh sections were checked by an optical microscope (Nikon Eclipse 90i, Japan) and mounted on double sided tape (Scotch, 3M 666, USA) bound to microscope glass slides, dried for 24 h, and stored at room temperature until analysis.

Laser ablation was performed using the laser system LSX-213 from Teledyne Cetac Technologies (Omaha, NE, USA) and the Photon Machines Analyte G2 ArF ablation system (Photon Machines, Redmond, USA). The commercial ablation cell from

Teledyne Cetac Technologies was replaced by a novel Peltier-cooled ablation cell built in-house, with lower washout times that improve the spatial resolution for imaging studies. Two different ICP-MS instruments were coupled to LA: a quadrupole instrument (model Agilent 7700cx; Agilent Technologies, Santa Clara, USA) and a double focusing ICP-MS (Element II) from Thermo Fisher Scientific (Bremen, Germany). Depending on the element of interest in the root sections as well as on its spectral interferences, LA-ICP-MS measurements were performed using two possible configurations. Thus, the study of Mn, Zn and Cu spatial distribution in rice roots sections was carried out with the ArF ablation system coupled to the quadrupole ICP-MS, while the analysis of Fe and Si was performed with the laser system LSX-213 coupled to the double focusing sector field ICP-MS. Determination of Fe and Si by ICP-MS suffers from important spectral interferences (e.g. $^{40}Ar^{16}O^{+}$, $^{40}Ca^{16}O^{+}$, $^{12}C^{16}O^{+}$, $^{14}N_2^{+}$, $^{14}N_2{}^{1}H^{+}$, etc.) and, therefore, ICP-MS was operated at medium mass resolution (R~4000) which is enough to obtain the total separation of polyatomic interferences in the determination of the sought isotopes (^{56}Fe, and ^{29}Si). Nonetheless, the signal intensity observed for ^{29}Si in the root sections was very low, and it was not possible to obtain two-dimensional images for this element.

Concerning ICP-MS instruments, torch position and ion lens voltage settings were optimized daily with a multi-elemental solution (including Li, Co, In, Y, Ce, and U) of 1 ng g^{-1} in 1% (w/w) HNO_3. Additionally, LA-ICP-MS coupling was also optimized daily using a SRM NIST 612 glass standard for high sensitivity, low background intensity, and $^{238}U/^{232}Th$ signal ratio close to 1 (to ensure a low fractionation effect due to the ICP ionization efficiency). $^{248}ThO/^{232}Th$ signal ratio was also measured for controlling oxide formation, being always below 2% and 20% (quadrupole and sector field ICP-MS instruments, respectively) at the selected conditions.

The root sections were ablated in scanning mode using a laser beam diameter of 10 µm. In this way, a two dimensional image that covers the whole section of the root was obtained to evaluate the different distribution of the elements in the structures of the tissue. Optimized analysis conditions for imaging of Cu, Mn, Zn and Fe in rice root sections from different supplementation treatments are summarized in Table 1. Two-dimensional images of elemental distributions were created using ImageJ-Fiji software. The concentration of the elements was not performed but the samples of all treatments

were analysed under same work conditions. Therefore, the signal intensity of each element may be directly correlated to the elemental concentration.

2.5. Histochemical staining of Fe with Prussian Blue stain formation

For the histochemical staining with Prussian Blue stain or ferrocyanide reaction, the Roschzttardtz et al., (2009) protocol was followed. Sections were infiltrated with equal volumes of 4% (v/v) HCl and 4% (w/v) K-ferrocyanide (Perls stain solution) for 15 min and incubated for 30 min at room temperature. Samples were washed with distilled water and observed in an Olympus Szx10 microscope (Fig. 3A-E), and photographs were taken using the Softimaging solutions software.

2.6. Scanning electron microscopy (SEM) and Energy Dispersive X-ray spectroscopy (EDX)

Plant material was analysed by SEM complemented with an energy dispersive X-ray analyser (EDX) following the protocol for elemental analysis and metallocalization study in plant material (de la Fuente et al., 2012). The organs and tissues analysed were roots (root hairs, iron plaque, epidermis, parenchyma, endodermis and vascular cylinder) and leaves (glandular trichomes, epidermis, and vascular cylinder). The root and leaf cross sections have been made at half of their length. An example of SEM-EDX analysis is shown in Fig. 3F-H. Samples were mounted onto conductive graphite stubs and sputters and gold-coated in a BIO-RAD SC 502 apparatus to ensure electrical conductivity and prevent charging under electron beams. Samples were examined with a Hitachi S-3000N (Japan) SEM using an acceleration voltage of 20kV and a working distance of 15 mm. Analyses were performed at room temperature. The qualitative element composition of samples was determined using an INCAx-sight with a Si-Li Detector (Oxford, England) with a detection limit of 10% of the main element. Three X-ray analyses were done for each cell layer to quantify the relative amount of Si and Fe.

2.7. Oxidative stress parameters

Enzymes were extracted from 0.1 g of 21 days-old intact frozen Fe-sufficient roots with 1 mL extraction solution, freshly prepared containing 50 mM potassium phosphate buffer at pH 7.8, 2 mM Na_2-EDTA, 10 mM DTT (1,4-Dithiothreitol), 20 mM ascorbic acid, 0.6% PVPP (polyvinyl polypyrrolidone) and 50 µl protease inhibitors cocktail.

The extracts were centrifuged at 14,000 × g for 15 min at 4°C. Total superoxide dismutase activity (SOD; EC 1.15.1.1) was assayed according to Giannopolitis and Ries (1977). One unit of SOD activity was defined as the amount of enzyme that causes 50% NBT reduction by superoxide radicals. Catalase activity (CAT, EC 1.11.1.6) was measured by monitoring the decrease in absorbance at 240 nm as a consequence of H_2O_2 consumption (Aebi, 1984). Total phenolic concentration was measured according to Ainsworth and Gillespie (2007) using Folin-Ciocalteu reagent.

2.8. Statistical analyses

Statistical analysis was carried out with SPSS (v. 24.0), using a Levene test for checking homogeneity of variances and ANOVA or Welch´s tests ($p < 0.10$). *Post hoc* multiple comparisons of means were carried out using Duncan´s test ($p < 0.10$) or Games-Howell´s test ($p < 0.10$).

3. Results

3.1. Silicon effect on micronutrient localization under Fe-sufficient conditions

Micronutrient localization was analysed in rice plants using two different approaches. The first consisted of the collection of a two dimensional (2-D) image for each element (Fe, Mn, Cu and Zn) using a laser ablation system coupled to an ICP-MS (Fig. 1, 2). In this way, it was possible to study the elemental distribution from a root cross section. The second approach consisted of the analysis of Fe concentration at different cell compartments of root and leaf cross sections using SEM-EDX (Table 2, Fig. 3). LA-ICP-MS results showed that $^{56}Fe^{+}$ was mainly localized in the outer layers, probably at the epidermis (iron plaque), with heterogeneous distribution. The signal intensity was higher when Si was applied, but Si did not affect Fe distribution (Fig. 1B). Also $^{56}Fe^{+}$ was localized in the vascular cylinder, but the signal intensity was low, and no differences were observed depending on Si supply. The SEM-EDX determinations showed that in root cross sections, Fe concentration was significantly higher in the root hairs, endodermis, and vascular cylinder when Si was not applied (Table 2). However, in the presence of Si, Fe concentration increased significantly in cells of epidermis and also increased, but not significantly, in the root surface forming the Fe plaque. In the

leaf cross sections, Fe concentration was significantly higher in the cells of the epidermis and the vascular cylinder when Si was not applied (Table 2).

Furthermore, oxidative stress parameters were analysed in roots (Fig. 4). Results showed a significant increase of SOD activity and total phenolic concentration after 14 days of Si supply, but CAT activity was not affected by Si addition.

The study of Mn, Cu and Zn distribution in root cross sections was only performed by LA-ICP-MS. The 2D-images obtained showed that all elements analysed were localized in the outer layers, probably in the epidermis and also in the vascular cylinder. The signal intensity of $^{55}Mn^{+}$, $^{63}Cu^{+}$ and $^{66}Zn^{+}$in the epidermis and in the vascular cylinder (excluding the emerged secondary root) of Fe-sufficient roots were lower when Si was added to the nutrient solution (Fig. 2B, 2C, 2D).

3.2. Silicon effect on micronutrients localization under Fe-deficient conditions

Results showed that $^{56}Fe^{+}$ was mainly localized in the outer layers, probably at epidermis, with a heterogeneous distribution (Fig 1C). The signal intensity was lower when Si was applied, contrary to what has been observed in plants grown with a normal Fe supply. Also $^{56}Fe^{+}$ was localized in the vascular cylinder, but the signal intensity was very low, and no differences were observed depending on Si supply (Fig. 1C), similar to what was observed in plants under Fe sufficiency. Moreover, the analysis of the Fe concentration (in percentage) at different cell compartments of root and leaf cross sections carried out by SEM-EDX showed that in the case of roots, the Fe concentration was significantly higher in the cells of the endodermis and the vascular cylinder when Si was applied. In root hairs and epidermis, no significant differences were obtained. In the case of leaves, there were no significant differences in the Fe concentration of the cell layers analysed with respect to Si supply (Table 2).

In Fe-deficient roots, the signal intensity of $^{55}Mn^{+}$ in the epidermis and in the vascular cylinder increased in an important way with Si application (Fig. 2B). When no Si was applied, the signal of $^{55}Mn^{+}$ was localized in spots along the epidermis. The application of Si led to an increase of the $^{63}Cu^{+}$ signal intensity in the vascular cylinder, but no differences with respect to Si addition were observed at the root epidermis (Fig. 2C). When Si was applied, it was observed that the signal intensity of $^{63}Cu^{+}$ increased in the

vascular cylinder. However, the signal intensity of $^{66}Zn^{+}$ in the epidermis and in the vascular cylinder did not change with Si application (Fig. 2D).

3.3. Effect of Si application and Fe status on micronutrients concentration

In Fe-sufficient roots (Fig. 5A), the Fe concentration increased significantly (by 4.5-fold), and the Mn concentration decreased significantly (by 2.6-fold) in -Si treatments compared to +Si treatments. The Cu and Zn concentrations were not affected by Si supply (Fig. 5A). The Fe deficiency caused significant increases in Mn, Cu and Zn concentration compared to Fe-sufficient plants. A comparison between the Si treatments showed that for Fe-deficient roots, the Fe concentration increased significantly (by 2-fold), and Mn concentration decreased significantly (1.6-fold) in -Si compare to +Si treatments. Similar to what happened under Fe sufficiency, the Cu and Zn concentrations in the root were not affected by Si supply under Fe deficiency.

Furthermore, the ratio shoot/root micronutrient concentration was calculated in rice plants to evaluate the effect of Si on the translocation of Fe, Mn, Cu and Zn to the shoot (Fig. 5B). The shoot/root concentration ratio showed that the Si supply significantly enhanced (by 4-fold) the Fe translocation from root to shoot in Fe-sufficient plants and by 1.6-fold in Fe-deficient plants. However, Si supply significantly decreased the Mn and Zn translocation in Fe-sufficient plants although Cu translocation was not affected. Under Fe deficiency, Mn, Cu and Zn translocation was not affected by Si supply.

The root apoplastic Fe concentration was significantly lower in the presence of Si independent of Fe status (Fig. 6A). Interestingly, in Fe-sufficient roots, the Fe apoplastic concentration decreased gradually in -Si, but it remained constant in +Si. Nevertheless, under Fe-deficient conditions the apoplastic Fe in +Si decreased more slowly than in -Si. The Fe concentration in the free Fe apoplastic root tissue (after washing the apoplastic Fe) was significantly higher in the presence of Si under Fe sufficiency, but in Fe-deficient roots, Si supply did not affect it (Fig. 6B).

3.4. Iron status effect on silicon distribution in rice plants

Si concentration (as a percentage) was analysed indifferent cell compartments using SEM-EDX (Table 2). In the roots of Fe-sufficient plants, no differences in the Si concentration were observed in the root hairs, endodermis and in the vascular cylinder

between Si treatments. Although, as expected, in iron plaque, epidermis and parenchyma Si concentration increased when Si was added to the nutrient solution. A similar situation was found in leaves, in which Si concentration increased when Si was added. Roots of Fe-deficient plants showed no differences in Si concentration in root hairs, iron plaque, endodermis and parenchyma between Si-treated and non-treated plants. On the other hand, Si concentration increased, as expected, in the root epidermis and vascular cylinder when Si was supplied, as well as in glandular trichomes, the epidermis and the vascular cylinder of leaves.

In the +Si treatments, Si concentration only increased in root parenchyma under Fe sufficiency and in the root vascular cylinder under Fe deficiency. In leaf, an increase in Si concentration was only found in the glandular trichomes under Fe deficiency. In the -Si treatments, Si concentration was higher in the epidermis and endodermis of the roots with Fe in the nutrient solution. No differences have been observed in leaf Si concentration related to the Fe nutrition of the plants.

4. Discussion

4.1. Silicon effect on micronutrient concentration and localization under Fe-sufficient conditions

Silicon application to the nutrient solution of rice plants affected the Fe concentration and localization in root and leaf in a different way depending on the Fe status. Under Fe sufficiency, Si supply favoured the Fe deposition in the root surface (iron plaque) on the epidermis (Fig.1, Fig. 3G, Table 2). Iron plaque is abundantly formed on root surfaces of common aquatic plants such as paddy rice (Wu et al., 2012). Moore et al., (2011) indicated that its formation occurred exclusively outside the exodermal cells, probably due to the blockage by the Casparian strip. The Fe distribution was not homogeneous along the epidermis; there were distinct regions of accumulation along the outer edge of the epidermis and along the boundary of the exodermis where entry is blocked. These authors also showed that Fe plaque is composed of fine needles approximately10 nm thick and 200 to 300 nm long, and this is why the Fe plaque does not appear as a sharp line in the nanoSIMS images (Moore et al., 2011). This fact was also evident in our study (Fig.3G), in which, using SEM-EDX analysis, a discontinuous Fe accumulation was detected along the root surface. The high standard deviation in Fe concentration

determined by EDX quantification of the Fe plaque also showed this heterogeneity (Table 2). Experimental results obtained by LA-ICP-MS also supported this fact, showing discontinuous spots in the outer layers (Fig.1B, C). However, the mechanism behind the uneven formation of Fe plaque is poorly understood. Moreover, previous studies demonstrated that there were many factors influencing the formation of Fe plaque, such as radial oxygen loss (ROL), genotype, pH, Eh and presence of microorganisms (Wu et al., 2012). Other factors, such as the presence of Si, can significantly increase Fe plaque formation (Wu et al., 2016). Fe plaque contains ferric hydroxides (63%), goethite (32%) and minor concentrations of siderite (5%), whose structure was characterized as amorphous or crystalline iron (oxyhydr) oxides. Iron oxides are able to combine with silicate to form iron silicate and deposit on root surfaces, or Si may precipitate as negatively charged silica particles in which Fe and other positive charge elements could be absorbed (Liu and Zhu, 2005). This would lead to the depletion of Fe and the rest of micronutrients from the solution (Liu and Zhu, 2005) and, therefore, the reduction in the micronutrient uptake into the plant (Howeler, 1973). Kirk and Bajita (1995) have demonstrated that Fe oxidation in the rice rhizosphere causes a substantial solubilisation of Zn from highly insoluble fractions in soil and that the solubilized Zn can be re-adsorbed by amorphous $Fe(OH)_3$.

LA-ICP-MS results presented here (Fig.1) showed that the $^{56}Fe^{+}$ signal intensity in the outer layers was higher when Si was applied, but Si did not affect Fe distribution. In our experimental conditions, iron was applied as Fe (III)-EDTA in the nutrient solution at a pH of 7.5. The low stability of this chelate at pH > 6.5 leads to Fe plaque formation. By contrast, Si supply decreased the Fe concentration in the root hairs, root endodermis, root vascular cylinder, leaf vascular cylinder and leaf epidermis (Table 2). These areas are directly related to Fe absorption and Fe transport inside the plant. As we mentioned above, the presence of Si increased the iron plaque on the root surface, possibly limiting the entry of Fe into the plant. A proposed hypothesis indicates that Si addition enhances the oxidation capacity of rice roots and therefore increases Fe precipitation in the growth media or at the root surface, forming the Fe plaque (Fu et al., 2012). The Fe plaque may acts as a barrier reducing the Fe uptake by the plant (Batty and Younger 2003). This hypothesis was supported by the lower Fe concentration in the root tissue (Fig. 5A) and in the root apoplast (Fig. 6A) of rice plants when Si was supplied under Fe-sufficient conditions (it should be taken into account that Fe plaque has been removed by acid-washing procedures, see Materials and Methods section). This

condition may activate Fe deficiency strategies in Fe-sufficient plants. An opposite Si effect on Fe absorption was observed in soybean plants (Gonzalo et al., 2013), where Si supply increased the Fe concentration in root and leaf tissue under Fe sufficiency. This shows the influence of plant species on Si effect on micronutrient absorption.

Total Fe concentration was subdivided into Fe concentration in the apoplast and Fe in the free apoplastic tissue after washing the apoplast. Si addition contributed to a decrease in the apoplastic Fe concentration in Fe-sufficient rice roots in comparison to –Si treatment, but maintained the apoplastic Fe concentration constant over time (Fig. 6A). However, when Si was not applied, the apoplastic Fe was gradually consumed. An opposite effect was observed under Fe sufficient conditions in cucumber plants, since Si addition increased the apoplastic Fe concentration in roots in comparison with -Si treatment (Pavlovic et al., 2013). The cation binding capacity of the apoplast cell walls can contribute significantly to this effect; further research is needed to clarify this finding and to compare the cell wall composition under +Si and –Si. On the other hand, Fe concentration on the apoplastic free root tissue (Fig. 6B) was significantly higher in the presence of Si under Fe sufficiency. This was correlated to the LA-ICP-MS images (Fig. 1B). Finally, a higher Fe translocation from root to shoot in Fe-sufficient plants (Fig. 5B) was obtained. Consistent with our results, Fu *et al.* (2012) reported that Si application in rice increased Fe transportation from root to shoot under Fe sufficiency. The proposed mechanisms that increase the Fe transport under Fe-sufficient conditions comprises Fe plaque formation that induced Fe deficiency under a normal Fe supply; the Fe deficiency mechanisms were activated, increasing the Fe transport to the shoot (Fig. 5B). The induction of Fe deficiency by Si was also supported by the increase of SOD activity (Fig. 4A) and total phenolic compounds (Fig. 4C) in root. Several authors have reported that Fe deficiency enhanced SOD activity in leaves of peach, *Medicago ciliaris*, maize and rape (M´sehli et al., 2014; Sun et al., 2007; Tewari et al., 2013), and also increased the phenolic accumulation in roots of red clover (Jin et al., 2007) and *Arabidopsis thaliana* (Siso-Terraza et al., 2016). Both parameters play an important role in protecting plants against oxidative damage caused by Fe deficiency.

Manganese, Cu, and Zn signal intensities were lower when Si was added to the nutrient solution (Fig. 2). These elements were localized mainly in the outer layers, probably in the cell walls of the epidermis which contain negatively charged sites that bind metal

ions (Sattelmacher, 2001). Also, these elements may be retained by the iron plaque due to adsorption or co-precipitation mechanisms (Liu and Zhu, 2005). Otte *et al.* (1989) and Zhang *et al.* (1998) suggested that an increase in the root surface covered with iron plaque (which is favoured by Si addition), diluted the global Zn concentration in plaque, which gave lower signal intensity. The same could be ascribed to Mn and Cu distribution.

Moreover, the Mn transporters (OsNramp5; OsMTP9) are localized in the plasma membrane of the epidermis and exodermis of rice roots (Sasaki et al., 2012), so a greater amount of this element is expected at these locations. Little is known about the molecular mechanisms for Zn and Cu uptake in rice (Sasaki et al., 2016). Under reducing conditions, Mn is maintained as soluble Mn^{2+}, but under ROL this Mn^{2+} should be oxidized to Mn^{4+} and precipitated as MnO_2 at the root outer layers. In the case of $^{63}Cu^{+}$ and $^{66}Zn^{+}$ elemental images, the signal intensity decreased in the vascular cylinder (Fig. 2C, 2D) when Si was applied.

4.2. Silicon's effect on micronutrients' concentration and localization under Fe-deficient conditions

Under Fe deficiency, Si supply significantly increased Fe concentration in endodermal and vascular cylinder cells of roots (Table 2) compared to the epidermal cells and root surface. Although the SEM-EDX analysis did not show significant differences in the percentage of Fe deposited in the root surface and in the epidermis depending on Si supply, elemental images obtained by LA-ICP-MS for $^{56}Fe^{+}$ indicated that the signal intensity of Fe in the outer layers of root decreased with Si application (Fig. 1C). Since no more Fe was added to the nutrient solution, Fe plaque formed during the Fe sufficient period could function as an Fe source on plant demand. Rice plants may release phytosiderophores (PS) to solubilize this Fe (III) from Fe plaque and take it up into the plant under Fe-deficient conditions. The chelation strategy is less sensitive to pH than the reduction strategy (Morrissey and Guerinot, 2009), so under our experimental condition (pH 7.5), the transport of Fe-PS appears to be predominant. Therefore, the plant responds to Fe deficiency increasing the phytosiderofore (PS) production that will allow solubilisation of the Fe plaque and translocation of the Fe to the shoot. The higher Fe translocation rate from root to shoot observed in rice plants with Si supply at Fe deficiency (Fig. 5B) may reduce the Fe concentration in the outer

layers. As observed in Fe-sufficient plants, the Fe distribution along the epidermis of rice roots was heterogeneous, showing spots of accumulation along the outer layer (Fig. 1C). Silicon supply decreased Fe concentration in root tissue (Fig. 5A) and in root apoplast (Fig. 6A), as occurred under Fe sufficiency. As such, the remaining iron plaque continued to act as a barrier reducing Fe uptake by the plant. An opposite Si effect on Fe absorption were observed in cucumber plants; since Si supply increased Fe concentration in leaf and root tissue, under Fe deficiency (Pavlovic et al., 2013; Bityutskii et al., 2013) attributed to a high amount of Fe in the root apoplastic pools when Si was added (Pavlovic et al., 2013). However, Si supply had no effect on root Fe concentration of Fe-deficient soybean plants (Gonzalo et al., 2013). The different responses observed in soybean, cucumber and rice suggest that the effect of Si in plants grown under iron deficiency was plant-specific. It should be noted that the total Fe concentration of Fe-sufficient rice roots was similar to the total Fe concentration of rice roots after four days of Fe deficiency in presence of Si (Fig. 5A). This may be explained by the fact that the rice roots were washed with 0.3 % HCl (v/v) before Fe determination such that the Fe plaque deposited in the root surface was removed.

From the viewpoint of plant mineral nutrition, the apoplast appears to be of interest since the mineral elements may be adsorbed or fixed to cell wall components which can serve as storage for nutrient acquisition. Silicon-supplied plants showed a significantly lower Fe concentration in the root apoplast, but the depletion of this Fe pool was slower than in -Si plants (Fig. 6A). Similar results were observed in cucumber, but after the first day of Fe deficiency, no differences regarding plant Si addition were observed (Pavlovic et al., 2013). This lower apoplastic Fe concentration observed in root with Si supply was accompanied by higher Fe translocation to shoot (Fig. 5B). By contrast, Pavlovic et al., (2013) found a significant decrease (about two-fold) in Fe root-to-shoot translocation rate in Fe-deficient cucumber when Si was applied. However, Si application in Fe-deficient cucumber increased the citrate concentration in the xylem sap. Indirect evidence for long distance organic ligand-assisted transport of metals has been extensively reported. Possible ligand candidates are a range of small molecules, including carboxylates such as citrate and malate, amino acids including nicotianamine, histidine, cysteine and PS (Alvarez-Fernandez et al., 2014).

Localization of Mn and Cu was also affected by Si supply under Fe-deficient conditions, increasing their signals not only in the outer layer but also in the vascular

cylinder in a significant manner (Fig. 2B, C). In +Si plants, the high $^{55}Mn^{+}$ signal intensity at the vascular cylinder (Fig. 2B) suggests the profusely described Fe/Mn antagonism; this effect was not relevant under Si deficiency. This may also be related to an increase in root to shoot translocation, not only for Fe, but for the rest of micronutrients favoured by Si. Moreover, the higher signal intensity for $^{55}Mn^{+}$ in the root outer layers also suggests the Fe deficiency induced higher Mn uptake (Fig. 5A). Regarding total metal concentration, it seems that the absorption of Mn, Cu, and Zn into the root was mainly influenced by Fe status, not by Si supply. Even Mn concentration in +Si was significantly higher, suggesting the blocking activity of the plaque on Fe uptake enhanced the antagonistic effect with Mn. The higher concentration of these metals in the root tissue in –Fe conditions (Fig.4A) was likely due to the increased abundance of the corresponding plasma membrane metal transporters (IRT1) or Fe-chelating compounds (PS) resulting from the deficiency of Fe which have a poor metal specificity and are capable of taking up other divalent metals in addition to the one involved in the deficiency (Morrissey and Guerinot, 2009). By contrast, Bityutskii et al., (2014) found that in Fe-deficient cucumber Si addition decreased Mn and Zn concentration in root and leaf tissues compared to –Si treatment, probably as a consequence of the increase of Fe due to the Si supply.

4.3. Iron status effect on silicon distribution in rice plants

Two transporters (Lsi1 and Lsi2) for Si uptake have been identified in rice (Ma et al., 2006; 2007). Lsi1 is responsible for the uptake of Si from soil into the root cells (influx transporter; Ma et al., 2006), and Lsi2 is responsible for the subsequent transport of Si out of the cortical cells towards the stele (efflux transporter; Ma et al., 2007). Lsi1 and Lsi2 are located in both endo- and exodermis cell layers of rice roots (Sasaki et al., 2016). They are mainly expressed in the mature zone of the root, but not in the root hairs (Ma et al., 2007; Yamaji and Ma, 2007; 2011). The SEM-EDX confirmed that in the roots of the plants treated with either Fe condition, no differences related to Si supply were observed in the root hairs, possibly because Lsi1 and Lsi2 were not expressed. These transporters are downregulated when Si is present in the media (Sasaki et al., 2016). On the contrary, differences related to Si supply were observed in the endodermis; in –Si plants, Si concentration in the endodermis (originally from the seed) was higher under Fe sufficiency, indicating a possible Fe modulation of Si transporters. In +Si plants , no differences were observed related to the Fe status as these transporters

were downregulated due to the presence of Si, and Fe did not seem to exert any influence on them. A similar situation has been found in Fe plaque, epidermis and in endodermis. Further research using genetic approaches would be necessary to confirm this.

5. Conclusions

A different Si effect was observed depending on plant Fe status. Under Fe sufficiency, Si supply increased Fe root plaque formation. This plaque acts as a barrier, reducing Fe uptake and, in turn, inducing Fe deficiency and oxidative stress signals in the plants. In contrast, Mn, Cu and Zn concentration in roots decreased when Si was added. Under Fe deficiency, +Si plants absorbed Fe from the plaque more efficiently than –Si plants; the previous activation of Fe deficiency strategies during the growing period (+Fe) decreased the Fe concentration in roots. However, Si supply significantly increased Mn uptake, clearly showing Fe/Mn antagonism, as well as the Cu concentration, suggesting a Fe/Cu antagonism, due to the non-specificity of transporters. In conclusion, as Si is an essential element for rice, special care should be taken to avoid crop losses due to a Si-induced Fe, Mn, Cu, and/or Zn deficiency.

Acknowledgements

Authors gratefully acknowledge the financial support by Spanish Ministry of Economy and Competitiveness projects: AGL2013-44474-R and RYC-2014-14985. Authors thank Miguel Suarez for help during the first LA-ICP-MS analysis, Prof. Carolina Escobar, PhD, from Universidad de Castilla-La Mancha for technical support in preparing the cross sections, Mª Carmen Marti and Lorena Selent for their assistance in phenol and enzymatic measurements, and Prof. Danika LeDuc, PhD, from California State University for her help in the English language editing.

References

Aebi, H.,1984. "[13] Catalase *in vitro*," in Methods in Enzymology (Academic Press), 121–126. doi:https://doi.org/10.1016/S0076-6879(84)05016-3.

Ainsworth, E. A., and Gillespie, K. M., 2007. Estimation of total phenolic content and other oxidation substrates in plant tissues using Folin-Ciocalteu reagent. Nat. Protoc. 2, 875–877. Available at: http://dx.doi.org/10.1038/nprot.2007.102.

Alvarez-Fernández, A., Díaz-Benito, P., Abadía, A., Lopez-Millan, A.-F., and Abadía, J., 2014. Metal species involved in long distance metal transport in plants. Front. Plant Sci. 5, 105. Available at: http://journal.frontiersin.org/article/10.3389/fpls.2014.00105.

Batty, L. C., and Younger, P. L., 2003. Effects of external iron concentration upon seedling growth and uptake of Fe and phosphate by the common reed, *Phragmites australis* (Cav.) Trin ex. Steudel. Ann. Bot. 92, 801–806. doi:10.1093/aob/mcg205.

Bienfait, H. F., van den Briel, W., and Mesland-Mul, N. T., 1985. Free space iron pools in roots. Plant Physiol. 78, 596. Available at: http://www.plantphysiol.org/content/78/3/596.abstract.

Bityutskii, N., Pavlovic, J., Yakkonen, K., Maksimović, V., and Nikolic, M., 2014. Contrasting effect of silicon on iron, zinc and manganese status and accumulation of metal-mobilizing compounds in micronutrient-deficient cucumber. Plant Physiol. Biochem. 74, 205–211. doi:http://dx.doi.org/10.1016/j.plaphy.2013.11.015.

de la Fuente, V., Rodríguez, N., and Amils, R., 2012. Immunocytochemical analysis of the subcellular distribution of ferritin in *Imperata cylindrica* (L.) Raeuschel, an iron hyperaccumulator plant. Acta Histochem. 114, 232–236. doi:http://dx.doi.org/10.1016/j.acthis.2011.06.007.

Fu, Y.-Q., Shen, H., Wu, D.-M., and Cai, K.-Z., 2012. Silicon-mediated amelioration of Fe^{2+} toxicity in rice (*Oryza sativa* L.) roots. Pedosphere 22, 795–802. doi:http://dx.doi.org/10.1016/S1002-0160(12)60065-4.

Giannopolitis, C. N., and Ries, S. K., 1977. Superoxide dismutases: I. Occurrence in higher plants. Plant Physiol. 59, 309–314. Available at: http://www.ncbi.nlm.nih.gov/pmc/articles/PMC542387/.

Gong, H. J., Randall, D. P., and Flowers, T. J., 2006. Silicon deposition in the root reduces sodium uptake in rice (*Oryza sativa* L.) seedlings by reducing bypass flow. Plant. Cell Environ. 29, 1970–1979. doi:10.1111/j.1365-3040.2006.01572.x.

Gonzalo, M. J., Lucena, J. J., and Hernandez-Apaolaza, L., 2013. Effect of silicon addition on soybean (*Glycine max*) and cucumber (*Cucumis sativus*) plants grown under iron deficiency. Plant Physiol. Biochem. 70, 455–461. doi:10.1016/j.plaphy.2013.06.007.

Hernandez-Apaolaza, L., 2014. Can silicon partially alleviate micronutrient deficiency in plants? A review. Planta 240, 447–458. doi:10.1007/s00425-014-2119-x.

Howeler, R.H., 1973. Iron-induced oranging disease of rice in relation to physicochemical change in a flooded oxisol. Soil Sci. Society America, Proceedings 37: 898-903.

Ishimaru, Y., Suzuki, M., Tsukamoto, T., Suzuki, K., Nakazono, M., Kobayashi, T., et al., 2006. Rice plants take up iron as an Fe^{3+}-phytosiderophore and as Fe^{2+}. Plant J. 45, 335–346. doi:10.1111/j.1365-313X.2005.02624.x.

Jin, C. W., He, X. X., and Zheng, S. J., 2007. The iron-deficiency induced phenolics accumulation may involve in regulation of Fe(III) chelate reductase in red clover. Plant Signal. Behav. 2, 327–332. Available at: http://www.ncbi.nlm.nih.gov/pmc/articles/PMC2634204/.

Kirk, G. J. D., and Bajita, J. B., 1995. Root-induced iron oxidation, pH changes and zinc solubilization in the rhizosphere of lowland rice. New Phytol. 131, 129–137. doi:10.1111/j.1469-8137.1995.tb03062.x.

Lanquar, V., Lelièvre, F., Bolte, S., Hamès, C., Alcon, C., Neumann, D., et al., 2005. Mobilization of vacuolar iron by AtNRAMP3 and AtNRAMP4 is essential for seed germination on low iron. EMBO J. 24, 4041–4051. doi:10.1038/sj.emboj.7600864.

Liu, W. J., and Zhu, Y. G., 2005. Iron and Mn plaques on the surface of roots of wetland plants. Acta Ecologica Sinica 25, 358-363

Lu, L., Tian, S., Liao, H., Zhang, J., Yang, X., Labavitch, J. M., et al., 2013. Analysis of metal element distributions in rice (*Oryza sativa* L.) seeds and relocation during germination based on X-Ray fluorescence imaging of Zn, Fe, K, Ca, and Mn. PLoS One 8, e57360. doi:10.1371/journal.pone.0057360.

Ma, J. F., Tamai, K., Yamaji, N., Mitani, N., Konishi, S., Katsuhara, M., et al., 2006. A silicon transporter in rice. Nature 440, 688–691. doi:http://www.nature.com/nature/journal/v440/n7084/suppinfo/nature04590_S1.html.

Ma, J. F., Yamaji, N., Mitani, N., Tamai, K., Konishi, S., Fujiwara, T., et al., 2007. An efflux transporter of silicon in rice. Nature 448, 209–212. doi:http://www.nature.com/nature/journal/v448/n7150/suppinfo/nature05964_S1.html.

Moore, K. L., Schröder, M., Wu, Z., Martin, B. G. H., Hawes, C. R., McGrath, S. P., et al. (2011). High-resolution secondary ion mass spectrometry reveals the contrasting subcellular distribution of arsenic and silicon in rice roots. *Plant Physiol.* 156, 913. Available at: http://www.plantphysiol.org/content/156/2/913.abstract.

Moore, K. L., Chen, Y., van de Meene, A. M. L., Hughes, L., Liu, W., Geraki, T., et al., 2014. Combined NanoSIMS and synchrotron X-ray fluorescence reveal distinct cellular and subcellular distribution patterns of trace elements in rice tissues. New Phytol. 201, 104–115. doi:10.1111/nph.12497.

Morrissey, J., and Guerinot, M. L., 2009. Iron uptake and transport in plants: the good, the bad, and the ionome. Chem. Rev. 109, 4553–4567. doi:10.1021/cr900112r.

M´sehli, W., Houmani, H., Donnini, S., Zocchi, G., Abdelly, C., and Gharsalli, M., 2014. Iron deficiency tolerance at leaf level in *Medicago ciliaris*; Plants. Am. J. Plant Sci. Vol.05 No.1, 13. doi:10.4236/ajps.2014.516268.

Otte, M.L., 1991. Heavy metal and arsenic in vegetation of salt marshes and floodplains. PhD Thesis, Vrije University, Amsterdam, The Netherlands.

Pavlovic, J., Samardzic, J., Kostic, L., Laursen, K. H., Natic, M., Timotijevic, G., et al., 2016. Silicon enhances leaf remobilization of iron in cucumber under limited iron conditions. Ann. Bot. 118, 271–280. doi:10.1093/aob/mcw105.

Pavlovic, J., Samardzic, J., Maksimović, V., Timotijevic, G., Stevic, N., Laursen, K. H., et al., 2013. Silicon alleviates iron deficiency in cucumber by promoting mobilization of iron in the root apoplast. New Phytol. 198, 1096–1107. doi:10.1111/nph.12213.

Roschzttardtz, H., Conéjéro, G., Curie, C., and Mari, S., 2009. Identification of the endodermal vacuole as the iron storage compartment in the Arabidopsis embryo. Plant Physiol. 151, 1329. Available at: http://www.plantphysiol.org/content/151/3/1329.abstract.

Sasaki, A., Yamaji, N., and Ma, J. F., 2016. Transporters involved in mineral nutrient uptake in rice. J. Exp. Bot. 67, 3645–3653. doi:10.1093/jxb/erw060.

Sasaki, A., Yamaji, N., Yokosho, K., and Ma, J. F., 2012. Nramp5 Is a major transporter responsible for manganese and cadmium uptake in rice. Plant Cell 24, 2155–2167. doi:10.1105/tpc.112.096925.

Sattelmacher, B., 2001. The apoplast and its significance for plant mineral nutrition. New Phytol. 149, 167–192. doi:10.1046/j.1469-8137.2001.00034.x.

Sisó-Terraza, P., Luis-Villarroya, A., Fourcroy, P., Briat, J.-F., Abadía, A., Gaymard, F., et al., 2016. Accumulation and secretion of coumarinolignans and other coumarins in *Arabidopsis thaliana* roots in response to iron deficiency at high pH. Front. Plant Sci. 7. doi:10.3389/fpls.2016.01711.

Sun, B., Jing, Y., Chen, K., Song, L., Chen, F., and Zhang, L., 2007. Protective effect of nitric oxide on iron deficiency-induced oxidative stress in maize (*Zea mays*). J. Plant Physiol. 164, 536–543. doi:https://doi.org/10.1016/j.jplph.2006.02.011.

Tewari, R. K., Hadacek, F., Sassmann, S., and Lang, I., 2013. Iron deprivation-induced reactive oxygen species generation leads to non-autolytic PCD in *Brassica napus* leaves. Environ. Exp. Bot. 91, 74–83. doi:10.1016/j.envexpbot.2013.03.006.

Wu, C., Ye, Z., Li, H., Wu, S., Deng, D., Zhu, Y., et al., 2012. Do radial oxygen loss and external aeration affect iron plaque formation and arsenic accumulation and speciation in rice? J. Exp. Bot. 63, 2961–2970. doi:10.1093/jxb/ers017.

Wu, C., Zou, Q., Xue, S.-G., Pan, W.-S., Huang, L., Hartley, W., et al., 2016. The effect of silicon on iron plaque formation and arsenic accumulation in rice genotypes

with different radial oxygen loss (ROL). Environ. Pollut. 212, 27–33. doi:http://dx.doi.org/10.1016/j.envpol.2016.01.004.

Yamaji, N., and Ma, J. F., 2007. Spatial distribution and temporal variation of the rice silicon transporter Lsi1. Plant Physiol. 143, 1306–1313. doi:10.1104/pp.106.093005.

Yamaji, N., and Ma, J. F., 2011. Further characterization of a rice silicon efflux transporter, Lsi2. Soil Sci. Plant Nutr. 57, 259–264. doi:10.1080/00380768.2011.565480.

Zhang, X., Zhang, F., and Mao, D., 1998. Effect of iron plaque outside roots on nutrient uptake by rice (*Oryza sativa* L.). Zinc uptake by Fe-deficient rice. Plant Soil 202, 33–39. doi:10.1023/A:1004322130940.

[colour Fig.]Fig. 1 Distribution of Fe obtained by LA-ICP-MS in a root cross section of rice grown in Fe-sufficient (+Fe) or Fe-deficient (-Fe) conditions with (+Si) or without (-Si) supply. (A) Optical image of the area analysed, (B) Qualitative distribution of $^{56}Fe^{+}$ along the root cross section, (C) Qualitative distribution of $^{56}Fe^{+}$ along the root cross section with a lower scale to emphasize the differences. The scale bar is in counts s^{-1}.

[colour Fig.]Fig. 2 Qualitative images obtained by LA-ICP-MS from the root cross section of rice grown in Fe-sufficient (+Fe) or Fe-deficient (-Fe) conditions with (+Si) or without (-Si) supply. (A) Optical image of the area analysed, (B) manganese ($^{55}Mn^{+}$), (C) copper ($^{63}Cu^{+}$), and (D) zinc ($^{66}Zn^{+}$). The scale bar is in counts s^{-1}.

[colour Fig.]Fig. 3 A selection of optical root tissues of rice stained with Perls blue: (A) apical young meristem, and root cross sections grown in (B) Fe- and Si-sufficient conditions (+Fe +Si), (C) Fe-sufficient and Si-deficient conditions (+Fe -Si), (D) Fe-deficient and Si-sufficient conditions (-Fe +Si) and (E) Fe- and Si- deficient conditions (-Fe -Si). Ep: epidermis; P: parenchyma; En: endodermis; Vc: vascular cylinder. A selection of the SEM images and EDX analysis after Perls staining of the Fe and Si concentration in: (F) root hair, (G) plaque, (H) vascular cylinder of the rice root grown in Fe- and Si- sufficient (+Fe+Si) conditions.

Fig. 4 Effect of Si supply on enzyme activities (A) SOD and (B) CAT, and (C) total phenolic concentration of Fe-sufficient rice roots grown with 1.5 mM H_4SiO_4 during 14 days. Data are means ± SE (n=3). Significant differences between treatments ($P < 0.05$) are indicated by different letters according to Duncan´s test.

Fig. 5 Effect of Si supply on Fe, Mn, Cu and Zn distribution within the plant tissue of rice grown in Fe-sufficient (+Fe) or Fe-deficient (-Fe) conditions. (A) Total concentration in root and (B) translocation factor (ratio shoot/root concentration). Data are means ± SE (n=3). Significant differences between treatments ($P < 0.10$) are indicated by different letters according to Duncan´s test.

Fig. 6 Fe concentration in (A) the root apoplast at day 1, 4 and 7 of Fe-deficiency and in (B) the apoplast root tissue at day 7 of Fe-deficient rice. The black line indicates growth without Si (-Si), the grey line with Si (+Si), the continuous line is Fe sufficient (+Fe),

and the dotted line Fe deficient (-Fe). Data are means ± SE (n=3). Significant differences between treatments ($P < 0.10$) are indicated by different letters according to Duncan´s test.

Tables

Table 1 Operating conditions of the ICP-MS and laser ablation instruments for imaging studies of rice roots sections

ICP-MS	**Thermo Element 2**	**7700cx ICP-MS**
RF Power	1330 W	1600 W
Cooling gas	15.5 L min^{-1}	15 L min^{-1}
Auxiliary gas	0.8 L min^{-1}	1.0 L min^{-1}
Nebuliser gas (Ar)	0.8 L min^{-1}	1.0 L min^{-1}
Cones	Ni (skimmer and sampler)	Ni (skimmer and sampler)
Isotopes	^{29}Si, ^{56}Fe	^{66}Zn, ^{63}Cu, ^{55}Mn
Sample time	5 ms	10 ms
Mass window	100%	-
Samples per peak	10	-
LA System	**LSX-213**	**Analytes G2 ArF**
Laser Energy	100% (~3.6 mJ)	100% (~7 mJ)
Repetition rate	5 Hz	15 Hz
Spot diameter	10 µm	10 µm
Scan speed	5 µm s^{-1}	5 µm s^{-1}
Ablation mode	single line scan	single line scan
Carrier gas (He)	1 L min^{-1}	0.9 L min^{-1}

Table 2 SEM-EDX analysis of the Fe and Si concentration (%) in the different cell layers of the rice root and rice leaf. Data are means ± SD (n=3). Significant differences between treatments ($P < 0.1$) within the same line are indicated by different letters.

			Fe-sufficiency		Fe-deficiency	
		%	+Si	-Si	+Si	-Si
Root	Root-hairs	Si	0.00 ± 0.00 a	0.04 ± 0.08 a	0.00 ± 0.00 a	0.06 ± 0.10 a
		Fe	1.56 ± 0.63 b	2.57 ± 0.94 a	1.74 ± 0.43 ab	0.54 ± 0.28 b
	Plaque	Si	0.30 ± 0.18 a	0.00 ± 0.00 c	0.18 ± 0.11 ab	0.07 ± 0.07 bc
		Fe	2.21 ± 1.53 a	0.98 ± 0.07 ab	1.70 ± 0.60 ab	0.00 ± 0.00 b
	Epidermis	Si	0.35 ± 0.12 a	0.20 ± 0.02 c	0.26 ± 0.07 ab	0.14 ± 0.03 d
		Fe	1.35 ± 0.31 b	0.67 ± 0.80 a	1.38 ± 0.49 b	0.60 ± 0.11 b
	Endodermis	Si	0.31 ± 0.11 ab	0.52 ± 0.24 a	0.29 ± 0.04 ab	0.21 ± 0.06 b
		Fe	1.25 ± 0.60 bc	5.44 ± 0.70 a	1.53 ± 0.39 b	0.50 ± 0.16 c
	Parenchyma	Si	0.28 ± 0.06 a	0.11 ± 0.04 b	0.08 ± 0.01 b	0.14 ± 0.04 b
		Fe	1.26 ± 0.19 a	1.10 ± 0.04 a	0.45 ± 0.05 b	0.43 ± 0.05 b
	Vascular cylinder	Si	0.16 ± 0.05 b	0.15 ± 0.05 b	0.31 ± 0.04 a	0.05 ± 0.09 b
		Fe	0.58 ± 0.27 b	2.16 ± 0.83 a	1.61 ± 0.64 a	0.27 ± 0.08 b
Leaf	Glandular trichomes	Si	6.78 ± 1.44 b	2.32 ± 0.42 c	12.43 ± 1.04 a	3.64 ± 0.27 c
		Fe	1.23 ± 0.20 a	0.92 ± 0.24 a	0.32 ± 0.10 b	0.17 ± 0.06 b
	Epidermis	Si	17.59 ± 4.62 a	1.06 ± 0.45 c	15.28 ± 5.21 a	0.58 ± 0.28 c
		Fe	1.01 ± 0.25 b	2.21 ± 0.76 a	0.00 ± 0.00 bc	0.15 ± 0.09 c
	Vascular cylinder	Si	1.98 ± 0.22 a	0.11 ± 0.13 b	1.67 ± 0.38 a	0.34 ± 0.14 b
		Fe	0.34 ± 0.17 b	1.99 ± 0.86 a	0.52 ± 0.05 b	0.32 ± 0.11 b

Fig. 1

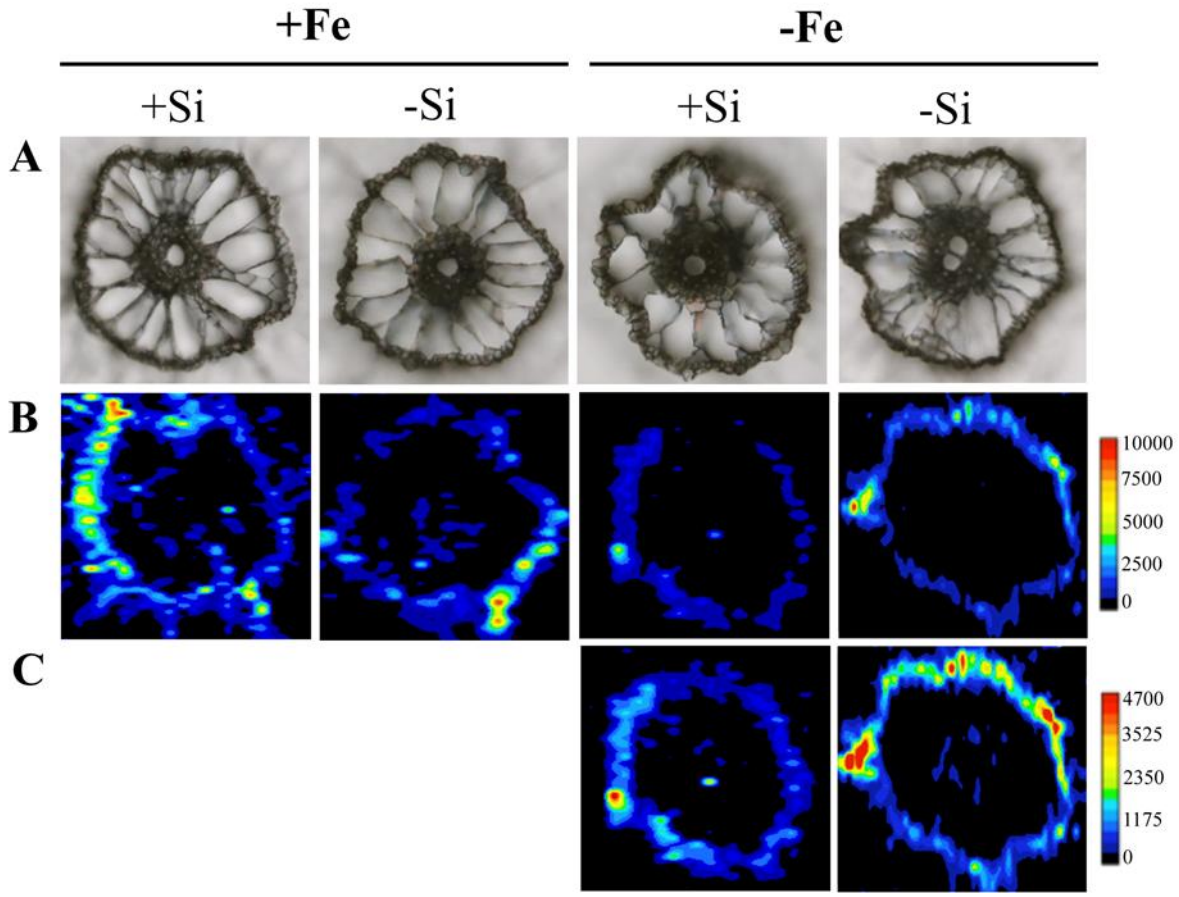
+Fe
-Fe
+Si
-Si
+Si
-Si
A
B
C
10000
7500
5000
2500
0
4700
3525
2350
1175
0

Fig. 2

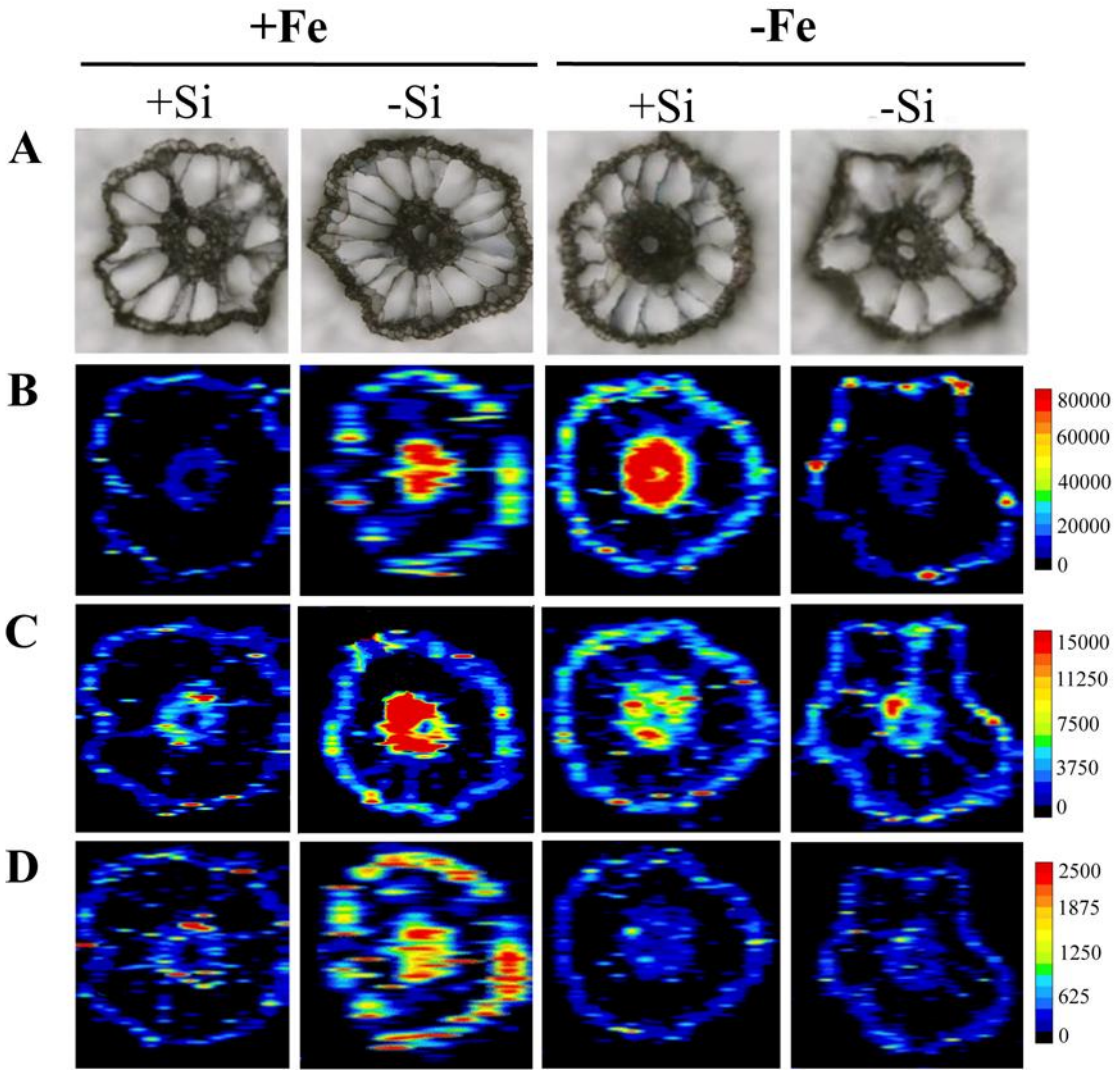
+Fe
-Fe
+Si
-Si
+Si
-Si
A
B
C
D
80000
60000
40000
20000
0
15000
11250
7500
3750
0
2500
1875
1250
625
0

Fig. 3

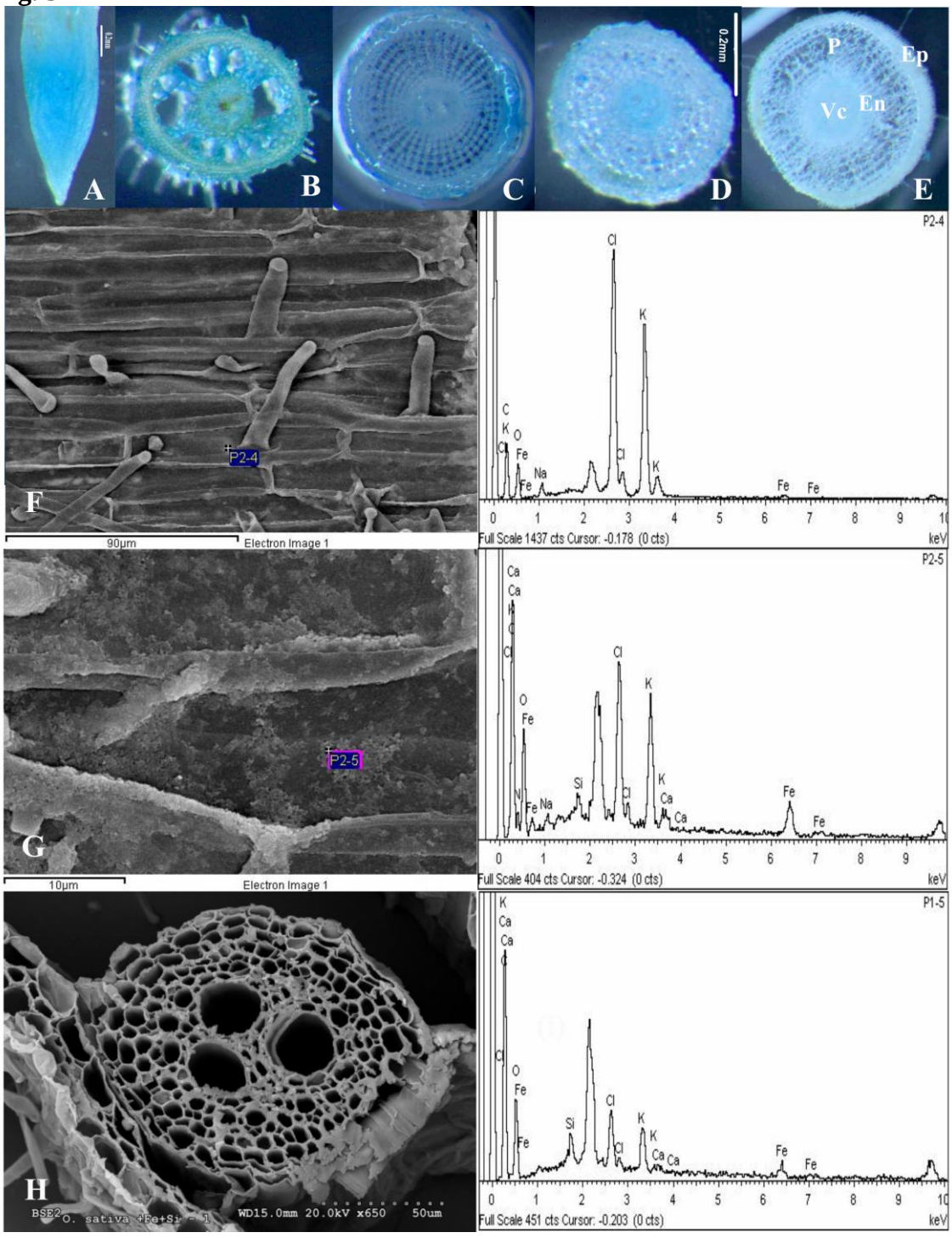
A
B
C
D
E
P
Ep
Vc
En
0.2mm
F
P2-4
90μm
Electron Image 1
Full Scale 1437 cts Cursor: -0.178 (0 cts)
keV
G
P2-5
10μm
Electron Image 1
Full Scale 404 cts Cursor: -0.324 (0 cts)
H
BSE2 O. sativa +Fe+Si - 1
WD15.0mm 20.0kV x650 50um
P1-5
Full Scale 451 cts Cursor: -0.203 (0 cts)

Fig. 4

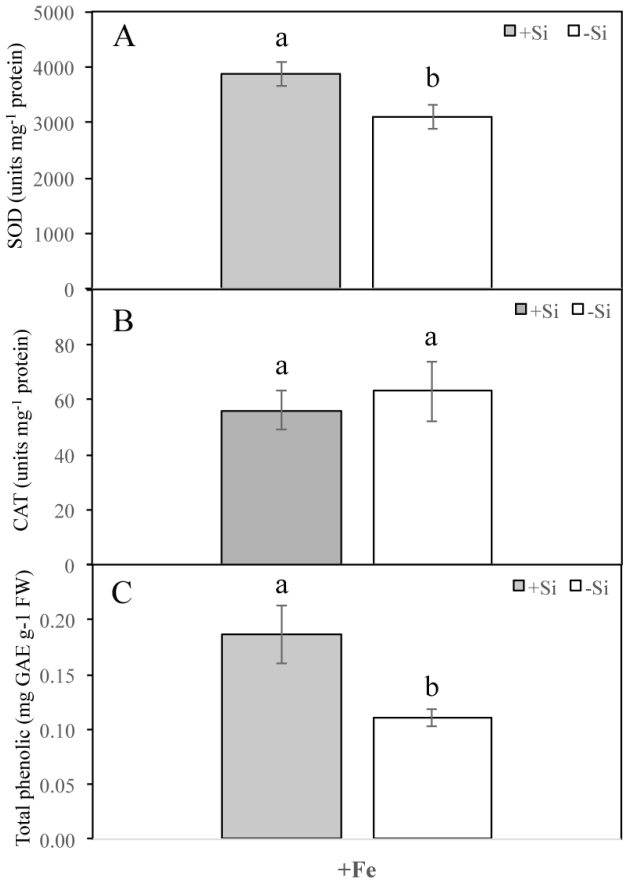
A
B
C
+Si
-Si
a
b
SOD (units mg-1 protein)
CAT (units mg-1 protein)
Total phenolic (mg GAE g-1 FW)
5000
4000
3000
2000
1000
0
80
60
40
20
0.20
0.15
0.10
0.05
0.00
+Fe

Fig. 5

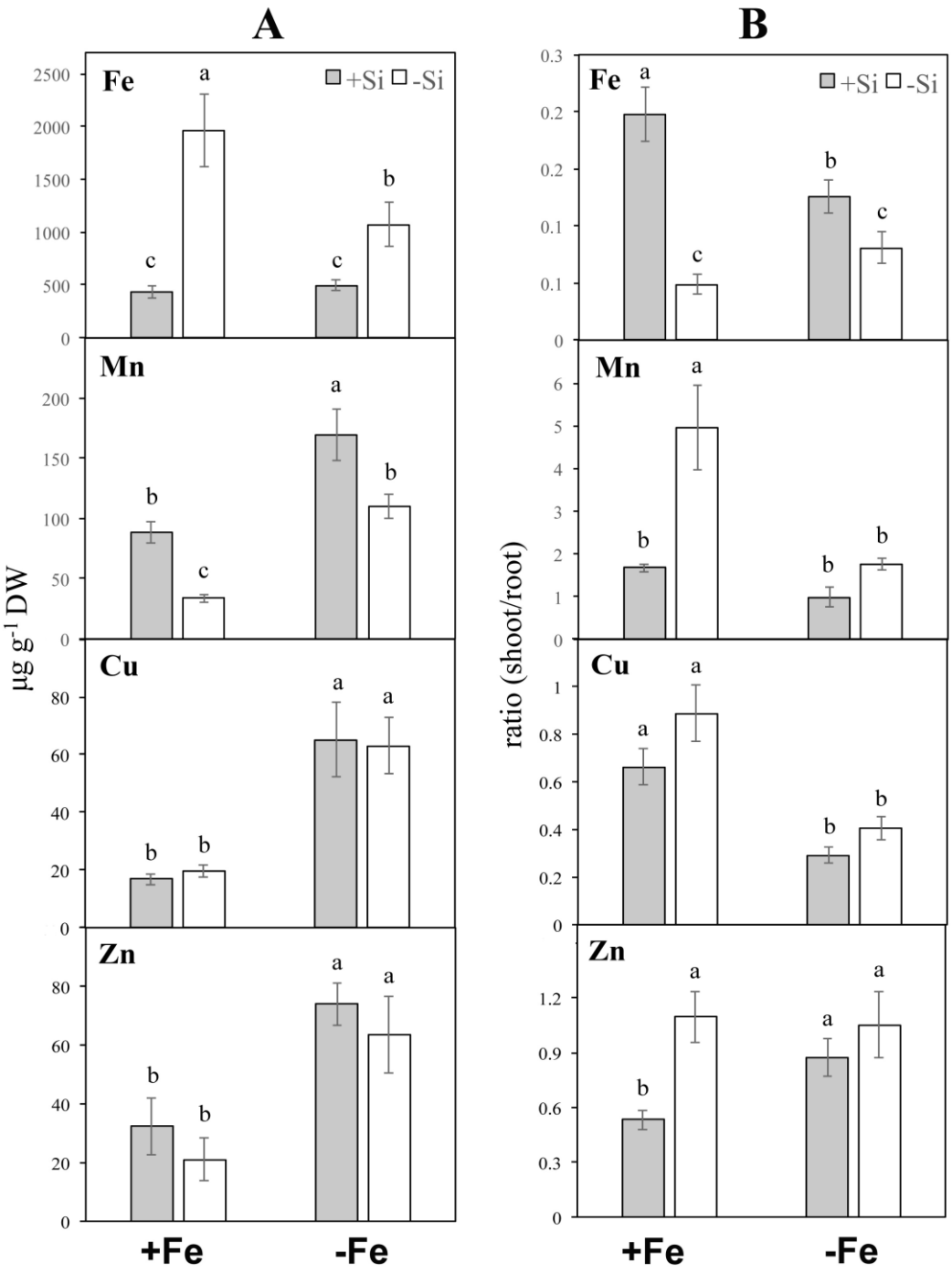

Fig. 6

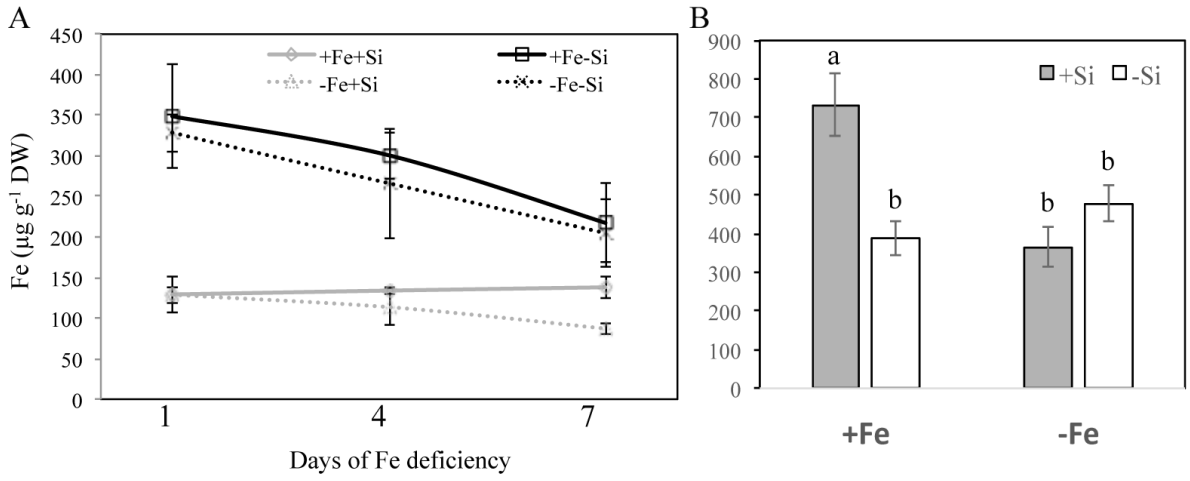
A
+Fe+Si
+Fe-Si
-Fe+Si
-Fe-Si
Fe (µg g-1 DW)
Days of Fe deficiency
B
+Si
-Si
a
b
b
b
+Fe
-Fe

CONTRIBUTIONS

SC-G carried out experiments, SR-M, BF and RP analysed samples by laser ablation; LH-A and VdF analysed samples by SEM-EDX; SC-G and LH-A planned research and wrote the paper.